Rare Metal Materials and Engineering
Volume 48, Issue 11, November 2019
Available online at www.rmme.ac.cn

Science Press

Cite this article as: Rare Metal Materials and Engineering, 2019, 48(11):3519-3526.

ARTICLE

Flow Behavior of Ultrafine Grain/Nanocrystalline γ-TiAl Based Alloys

Chen Hua, Pei Wen, Gong Xuebo, Duan Zhenxin

Changchun University of Technology, Changchun 130000, China

Abstract: Ultrafine grain/nanocrystalline two-phase γ-TiAl based alloy was prepared by high energy ball milling and vacuum hot pressing sintering. Ti, Al and Nb single powders were mixed together to make the nanocrystalline powder with a nominal composition of Ti-45Al-5Nb (at%). After ball milling, the nanocrystalline powder was sintered at the temperature of 1200 °C with the pressure of 30 MPa for 1 h. The sintered microstructure consisted of nanocrystalline α_2-Ti_3Al and the equiaxed γ-TiAl with grains less than 500 nm. The hot compressive flow behavior of Ti-45Al-5Nb alloy was studied by the Gleeble-1500D thermal simulator at deformation temperatures of 1100, 1150 and 1200 °C and strain rates of 1×10^{-4}, 1×10^{-3} and 1×10^{-2} s^{-1}. The results reveal that the peak stresses of equiaxed ultrafine microstructure are significantly lower than that of the alloys with micron-scale structure. The value of peak stress is reached at the early stage of compression (2.5%~3% strain), and the flow stress decreases with the increase of temperature and decreasing strain rate. A constitutive equation was established based on experimental data which reflects the structural characteristics of the alloy during hot deformation. It shows that the deformation mechanisms are mainly intracrystalline dislocation in γ-TiAl phase and intergranular twins in γ/γ (001).

Key words: γ-TiAl alloy; ultrafine grain/nanocrystalline; hot compression; constitutive equation

Compared with traditional Ti-based alloys and Ni-based superalloys, two-phase γ-TiAl based alloy (γ-TiAl+α_2-Ti_3Al) has superior performance for high-temperature applications based on low density (less than 4.5 kg/cm^3), excellent strength and good oxidation resistance at elevated temperatures[1-3]. However, the alloy exhibits poor plasticity at room temperature. Plastic deformation is difficult below 700 °C, which limits the practical application[4,5].

Recently, Chen et al.[6] studied the single crystal structure of γ-TiAl in Ti-45Al-8Nb alloy and the room-temperature plasticity reached 3% which was the highest plasticity indicator for γ-TiAl alloy. Meanwhile, some studies have shown that the plasticity of two-phase Ti_3Al and TiAl microstructures might be higher than that of single phase TiAl [7,8]. Kad et al investigated the interface state of γ-TiAl and Ti_3Al in the lamellar structure of Ti-48Al-2Cr alloy, and found coherent stress and high dislocation density at the γ/γ interface, which had great inspiration for the study of the deformation and fracture of the lamellar TiAl alloys[9-11].

Many investigations have been done on the mechanical properties of TiAl-based alloy and the effects of hot deformation and recrystallization treatment, which verified that grain refinement could improve their strength and plasticity[10-13]. Yamaguchi et al and Kishida et al[14,15] proposed that the mechanism of deformation of TiAl-based alloy was dislocation and twinning, and the shape change of the deformed grains could cause significant stress, resulting in superplastic dislocation at the interface.

At present, the research on two-phase γ-TiAl based alloy (TiAl+Ti_3Al) is mainly carried out in lamellar microstructures, while the study of two-phase equiaxed alloy is rarely reported.

In the previous study, the research team found that the powder metallurgy (PM) technique is the best way to obtain

Received date: November 25, 2018
Foundation item: National Natural Science Foundation of China (51371038)
Corresponding author: Chen Hua, Ph. D., Professor, College of Materials Science and Engineering, Changchun University of Technology, Changchun 130000, P. R. China, Tel: 0086-431-85716396, E-mail: chenhua@ccut.edu.cn

two-phase equiaxed γ-TiAl based alloy[16,17]. Moreover, this method has a great advantage for large-scale production of low-plasticity materials. Forming requirements of the parts of the complex shape can be met through further hot pressing deformation. The γ-TiAl and α_2-Ti_3Al phase can be synthesized in the range of Ti-(45-48)Al, and the main difference of the material is the proportion of two phases. This paper mainly discusses the Ti-45Al-5Nb (at%) alloy. And adding alloy element Nb is considered to be the most beneficial method for improving the workability and high-temperature strength of TiAl -based intermetallic[18].

In this paper, the microstructures of γ(TiAl) and α_2(Ti_3Al) two-phase equiaxed ultrafine grain/nanocrystalline alloy was synthesized by high-energy ball milling and vacuum hot pressing sintering. Through hot compression tests, this study investigated the relationship among the flow stress, temperature, strain rate, and strain of the microstructure are investigated and the deformation mechanisms evolution and the effects of ultrafine grain/nanocrystalline structure on deformation behavior were also discussed. The results would provide theoretical and experimental basis for the equiaxed γ-TiAl based alloy of the hot deformation process.

1 Experiment

In order to obtain γ-TiAl+α_2-Ti_3Al two-phases, the alloy composition in this study was Ti-45Al-5Nb. Ti powder (average particle size >50 μm, purity >99%), Al powder (average particle size >75 μm, purity >99%) and Nb powder (average particle size >75 μm, purity >99%) were mixed together to make the powder with a nominal composition of Ti-45Al-5Nb (at%). The mixed powder was milled for 25 h by three dimensional high-energy pendular ball milling in argon atmosphere (milling speed 550 r/min). The mass ratio of steel balls to mixed powder is 10:1, and the steel balls were made of GCr15 (GB), having two different diameters of 10 and 15 mm. The process of powder ball grinding and canning was carried out under the protection of argon gas. Anhydrous ethanol was used as the process control agent to reduce the impurities brought by ball grinding. Subsequently, the specimens with a relative density of approximately 97% were prepared at 1200 °C for 1 h by ZT-40-20Y vacuum hot pressing sintering furnace (pressure 30 MPa). The resulting microstructure consisted of the equiaxed γ-TiAl with grains less than 500 nm and nanocrystalline Ti_3Al.

Compressive tests were conducted on a computer-controlled (Gleeble-1500D) thermal-mechanical simulator at 1100, 1150 and 1200 °C with strain rates 1×10^{-2}, 1×10^{-3} and 1×10^{-4} s^{-1}, respectively. The degree of compression deformation was 30%. Cylindrical specimens with dimensions of Φ8 mm×12 mm were cut from the sintered bulk by electric discharge machining. The morphology of specimens before and after hot compression deformation are shown in Fig.1. The surfaces of the samples are smooth, and no cracking phenomenon occurs. The step-by-step procedures are shown in Fig.2. Microstructure and morphology of the sintered and vertical sections of hot compressed samples were analyzed by transmission electron microscopy (TEM, JEM-2000EX) operated at 100 kV and high-resolution electron microscope (HREM, FEI Talos F20S), respectively by standard metallographic procedures.

2 Results and Discussion

2.1 Analysis of microstructure under compression

The X-ray diffraction pattern of ball milled powder does not find oxide element in Fig.3. Fig.4 shows the sintered microstructure. As expected, the microstructure is composed of equiaxed γ-TiAl phase and nanocrystalline α_2-Ti_3Al phase, which has been identified by the diffraction pattern (Fig.4 inset). The size of the γ-TiAl phase is about 500 nm. In addition, the regular polygonal grain boundaries can be found, indicating that the sintered microstructure is compacted. According to phase diagrams and references, phase transformations occurred in the 1100~1200 °C.

Generally, TiAl Alloy are synthesized by mixed powder reaction sintering, so the sintering organization is greatly influenced by the homogenization of powders. If the pow-

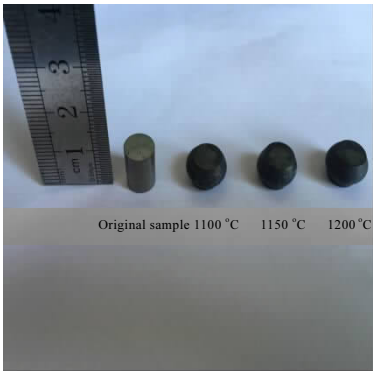

Fig.1 Specimens before and after hot compression deformation

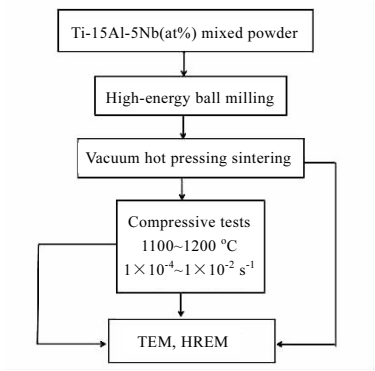

Fig.2 Step-by-step procedures for sample preparation and characterization

ders can not achieve homogenization diffusion at high temperature with short period of time, the enrichment phenomenon of the elements may occur. The Ti-rich field may form high temperature β phase, and B_2 phase will be formed during cooling. This in homogeneous powders often formed lamellar structure[19].

In this study, the homogeneous nanoscale powders were obtained by high-energy ball milling. Therefore, the powders diffused rapidly during sintering and form the ultrafine/equiaxed γ-TiAl and α_2 two-phase different from the lamellar structure. B_2 phase was not found in the sintered and compressed structure. TEM (Fig.4) and XRD pattern (Fig.5) of the sintered microstructure further confirmed that TiAl and α_2 phase are formed after sintered at 1200 °C.

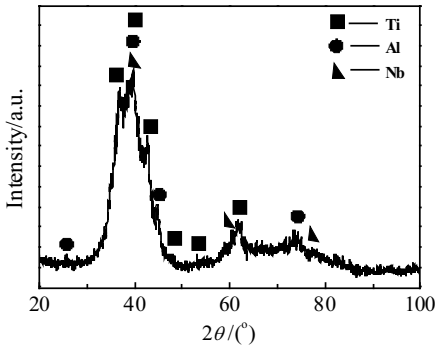

Fig.3 XRD pattern of ball milled powder for 25 h

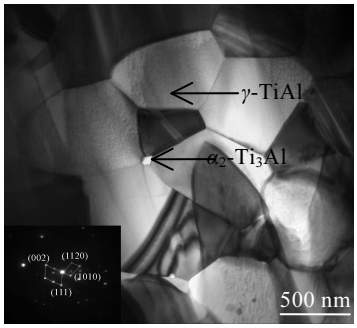

Fig.4 TEM image of the sintered microstructure

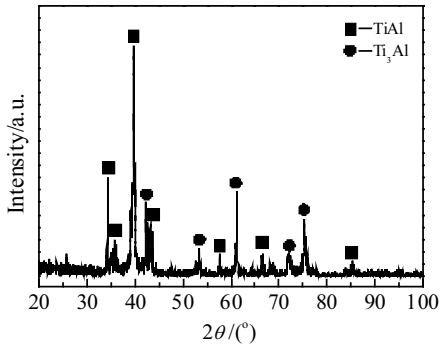

Fig.5 XRD pattern of the sintered microstructure

Fig.6 shows the microstructures of the compressed samples at 1100 and 1200 °C with three strain rates of 1×10^{-2}, 1×10^{-3} and 1×10^{-4} s^{-1}. After the compressive test, the samples were immediately quenched in water to retain the microstructure under the compressed state.

At 1100 °C with the highest value of strain rate 1×10^{-2} s^{-1}, the original equiaxed γ-phase grains have a slight plastic deformation and dislocation pile-ups in the grain boundary and intragranular γ phase (Fig.6a). At the strain rate of 1×10^{-3} s^{-1}, the deformation dislocations network is also observed in the grains, and the arrows indicate the deformation direction (Fig.6b). For the deformed grains, the diffraction pattern indicates the γ phase. The further analysis indicates that the plastic deformation mainly occurs in γ-TiAl matrix phase. Due to the climbing and slipping of the dislocation, γ-TiAl grains are more easily deformed. However, the α_2-Ti_3Al phase is situated at the boundary of the γ phase, and shows no obvious plastic deformation. Due to the fine grain size and little slip system, α_2-Ti_3Al phase may shift with the deformation of γ-TiAl phase. When the strain rate decreases to 1×10^{-4} s^{-1}, the twin phenomenon is observed in the γ grain, and the twin stripe is clear and distinct (indicated by the arrows in Fig.6c). This is because one crystal lattice along the grain will rotate to form a mirror symmetrical twin when the shear stress on the grain reaches a certain stage during the compression. With the decrease of strain rate, the dislocation deformation develops into dislocation and twins deformation, and then the degree of the grains deformation increases significantly.

At 1100 °C with the highest value of strain rate 1×10^{-2} s^{-1}, the original equiaxed γ-phase grains have a slight plastic deformation and dislocation pile-ups in the grain boundary and γ phase intragranular (Fig.6a). At the strain rate of 1×10^{-3} s^{-1}, the presence of deformation dislocations network is also observed within the grains, and the arrows indicate the deformation direction (Fig.6b). Compared with the sintering structure (Fig.4), the dislocation increases obviously and the deformation occurs. At this time, compared with the Fig.6a and 6b, many grains in Fig.6c have become elongated and form deformation dislocations and twin sub-structures, indicating that the microstructure is in a dynamic recovery state. As the thermal deformation progresses, the dynamic recovery makes the dislocation density decrease and leads to softening. This softening effect is greater than work hardening by plastic deformation. At this time, the dynamic recovery occurs. Under the 1200 °C and 1×10^{-2} s^{-1} deformation conditions, most of the grains are only slightly deformed due to the rapid strain rate (Fig.6d). When the strain rate is 1×10^{-3} s^{-1}, the dislocation cells and high dislocation density in the microstructure can be observed (indicated by the arrow in Fig.6e). When the strain rate is 1×10^{-4} s^{-1}, a mass of dislocations is formed in the microstructure (indicated by the arrow in Fig.6f). And the

dislocation density is higher in the grain boundary regions than the grain interiors (intragranular zone).

Fig.6g shows the HREM image of a trigeminal grain boundary obtained at 1100 °C and 1×10^{-4} s^{-1}. Electron beam is parallel to the γ phase (111) plane for incidence, confirming the α_2/γ interface is composed of $(20\bar{2}2)\alpha_2$ and$(111)_\gamma$. Fig. h shows the twinning of the γ/γ interface, as indicated by the arrow in Fig.6c, which is combined with crystal surface (001) at an angle of 110.22°. It is shown that the dislocation slip and twins coordinate deformation at high temperature and low strain rate. The deformation mechanisms of the equiaxed ultrafine Ti-45Al-5Nb alloy are dislocations and twins.

2.2 True stress-strain curves

Fig.7 shows the true stress-strain curves at different temperatures and strain rates. All curves exhibit initial strain hardening after yielding, and a peak stress at a low true strain (<0.03), followed by a moderate and continuous strain softening until a steady state is approached in the temperature range of 1100~1200 °C. As the deformation temperature increases, the value of peak stress decreases. At the initial stage of deformation, Since high density dislocations are accumulated under fast strain rate, the work hardening has the dominant effect. With the increase of deformation degree, the diffusion capacity of atoms at high temperatures is enhanced, the ability of dislocation to overcome obstacles is improved. When the stress reaches a peak value, the softening effect begins to be dominant with the acceleration of dynamic recovery and recrystallization, and the stress-strain curves approach a steady state[20].

At a lower strain rate (1×10^{-4} s^{-1}), the steady state flow is reached at a much reduced strain level. As shown in Fig.7c, the peak stress is 52 MPa at 1100 °C, while only 30 MPa at 1200 °C, which are almost consistent with the steady-state stress value. It shows that when the strain rate is low, the plastic deformation capacity of the alloy can be greatly improved[21]. Compared to the two-phase γ-TiAl alloy with the micron-scale structure, the peak stress values of equiaxed ultrafine microstructure are significantly lower[22,23], the peak stress is reduced by almost 30%, and the peak stress is reached at the early stage of compression (2.5%~3% strain). The two-phase alloy with the micron-scale structure reach the peak stress under the condition of 77 MPa, 1200 °C.

In general, the work hardening of the polycrystal is mainly due to the non-coherent boundaries, which hinder the movement of dislocations. With the decrease of grain size and the increase of the grain boundary, the plastic deformation will be more difficult to proceed and the strength will be higher. However, a smaller grain size means a higher coordination deformation ability of the grain boundary. Hence, compared to the micron-scale structure, the fine grain structure is more conducive to the grain slip and deformation during hot compression process, and the work-hardening ability is reduced at a certain temperature and strain rate. The peak value of flow stress is significantly reduced in ultrafine equiaxed grains structure, which indicates that the ultrafine equiaxed grains are favorable for the hot forming under low stress level.

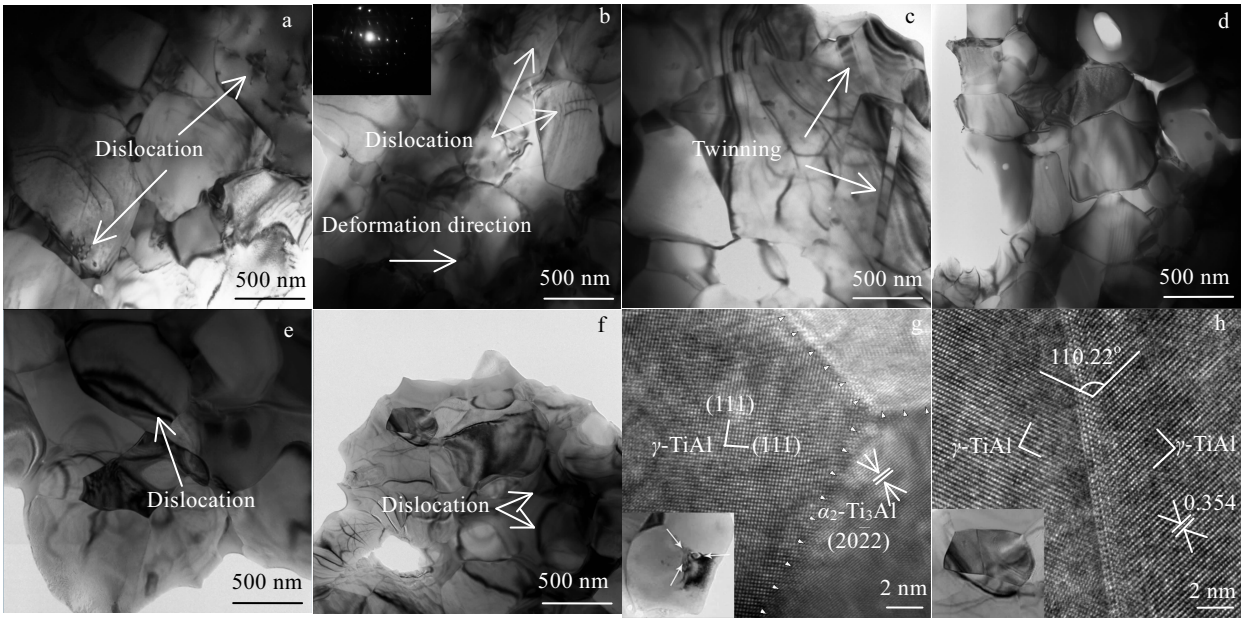

Fig.6 TEM images of deformed microstructures obtained under different conditions: (a) 1100 °C, 1×10^{-2} s^{-1}; (b) 1100 °C, 1×10^{-3} s^{-1}; (c) 1100 °C, 1×10^{-4} s^{-1}; (d) 1200 °C, 1×10^{-2} s^{-1}; (e) 1200 °C, 1×10^{-3} s^{-1}; (f) 1200 °C, 1×10^{-4} s^{-1}; (g) HREM image of a trigeminal grain boundary at 1100 °C, 1×10^{-4} s^{-1}; (h) HREM image of the amplified γ/γ grain boundary at 1200 °C, 1×10^{-4} s^{-1}

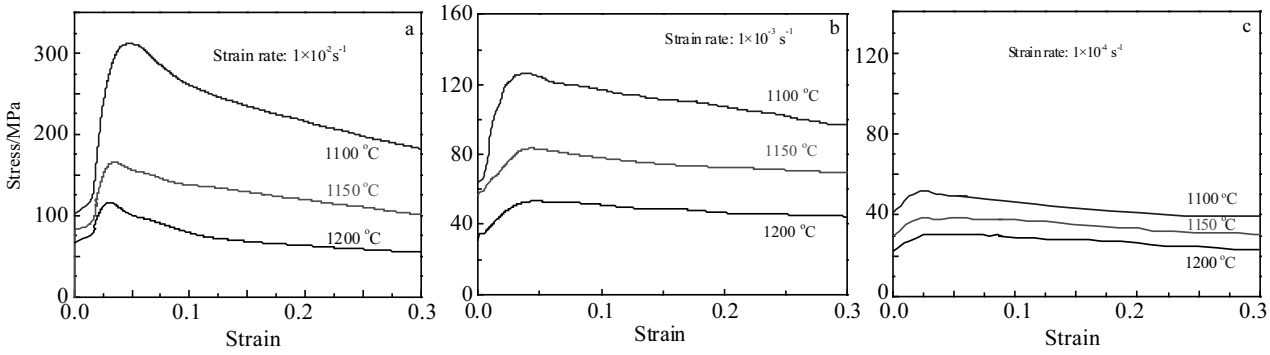

Fig.7 True stress-strain curves at different strain rates and temperatures: (a) 1×10^{-2} s^{-1}, (b) 1×10^{-3} s^{-1}, and (c) 1×10^{-4} s^{-1}

2.3 Recrystallization regional diagram

The steady-state strain is obtained according to the first inflection point or the stress at the steady state on the stress-strain curve. Dynamic recrystallization kinetics can be described by the following equation. The relationship between the strain ε_p and the critical strain ε_c of dynamic recrystallization is shown in Eq.(1) :

$$\varepsilon_c=0.8\varepsilon_p \quad (1)$$

As shown in Table 1, according to the strain corresponding to the peak stress, the critical strain of dynamic recrystallization and steady-state strain value of dynamic recrystallization were calculated by Eq.(1).

It can be seen from Table 1 that when the strain rate is 1×10^{-2} s^{-1}, the critical strain of dynamic recrystallization is between 0.02 and 0.04. When the strain rate is 1×10^{-3} s^{-1}, the critical strain of dynamic recrystallization is between 0.029 and 0.04. When the strain rate is 1×10^{-4} s^{-1}, the critical strain of dynamic recrystallization is the smallest, about 0.2.

As observed in Fig.8, the critical strain of dynamic recrystallization is between 0.02 and 0.04 and the steady-state strain of dynamic recrystallization is between 0.1 and 0.3. With the increase of deformation temperature, the critical deformation required to complete dynamic recrystallization decreases gradually.

2.4 Constitutive equation

True stress-strain curves describe a comprehensive overview of the dynamic hardening and softening effects in the process of compression. The flow stress constitutive equations are useful because they provide valuable insights to the structure character of the material in the flow process. Historically, this equation was derived from creep equation that takes into account a steady state, which was shown by Sellars and Tegart, using the hyperbolic sine function suggested by Garofalo, in which hot working could be considered as a thermally activated process and it could be described by strain rate equations similar to those employed in creep studies[24,25]. The constitutive equation is introduced

Table 1 Critical strain and steady-state strain of dynamic recrystallization

Strain rate/s^{-1}	Strain	1100 °C	1150 °C	1200 °C
1×10^{-2}	ε_p	0.045	0.031	0.027
	ε_c	0.036	0.0248	0.0216
	ε_s	0.3	0.28	0.22
1×10^{-3}	ε_p	0.037	0.043	0.046
	ε_c	0.0296	0.0344	0.0368
	ε_s	0.23	0.18	0.13
1×10^{-4}	ε_p	0.026	0.026	0.03
	ε_c	0.0208	0.0208	0.024
	ε_s	0.188	0.163	0.128

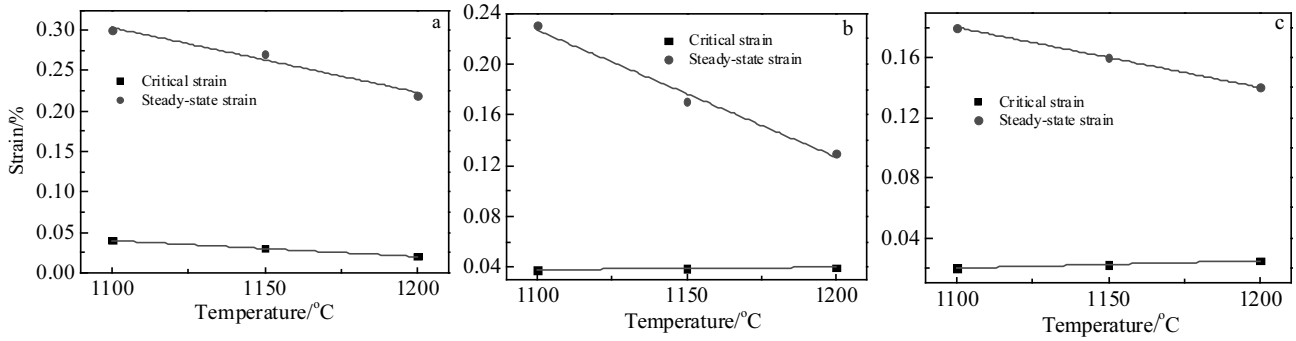

Fig.8 Recrystallization regional diagram at different strain rates: (a) 1×10^{-2} s^{-1} , (b) 1×10^{-3} s^{-1}, and (c) 1×10^{-4} s^{-1}

to develop the relationship between temperature and strain rate. And it explains the flow behavior of materials during deformation as a thermally activated process and is expressed as Eq.(2).

$$Z = \dot{\varepsilon}\exp(Q/RT)=A[\sinh(\alpha\sigma)]^n \quad (2)$$

Here, Z is Zener-Hollomon parameter. σ, $\dot{\varepsilon}$, Q and T denote the flow stress, strain rate, deformation activation energy and thermal dynamic temperature, respectively. R denotes the molar gas constant [8.314 J·(mol·K^{-1})].

The following are the constitutive equations for all stress level, low stress and high stress level. The equations can be used to describe the hot deformation behavior of materials.

$$\dot{\varepsilon} = A[\sinh(\alpha\sigma)]^n \exp(-Q/RT) \quad (3)$$

$$\dot{\varepsilon} = A_1\sigma^{n_1} \quad (4)$$

$$\dot{\varepsilon} = A_2\exp(\beta\sigma) \quad (5)$$

In the formulas, A, A_1, A_2, α and β are material constants, n_1 and n are stress exponents. The relationship between α, n and β is: $\alpha\approx\beta/n$. The parameters α, n, and Q associated with the peak stress were evaluated using a method similar to that of Uvira and Jonas[26]. It consists of varying α so as to minimize the standard deviation associated with fits to Eq.(3).

Taking the logarithms of the two sides of Eqs.(3)~(5), Eqs. (6)~(8) are derived.

$$\ln\dot{\varepsilon} = \ln A + (-Q/RT) + n\ln[\sinh(\alpha\sigma_p)] \quad (6)$$

$$\ln\dot{\varepsilon} = \ln A_1 + n_1\ln\sigma \quad (7)$$

$$\ln\dot{\varepsilon} = \ln A_2 + \beta\sigma \quad (8)$$

It is assumed that peak stress σ_p and strain rate $\dot{\varepsilon}$ meet the exponential relationship and hyperbolic sine relationship. The exponential and the power exponential relation curves between the peak flow stress and strain rate in the form of $\ln\dot{\varepsilon}$-$\ln\sigma_p$ and $\ln\dot{\varepsilon}$-σ_p are expressed in Fig.9. A tentative range of α value is selected on the basis of the material constants determined for γ-TiAl alloy deformed by hot compression. Based on the formula $\alpha\approx\beta/n$, the final value of α is selected by calculating the effect on n of variations in α over the above narrow range. The most suitable value of α is the one which led to the minimum standard deviation in n over the full range investigated, and the parameter α is 0.0013.

Eq.(9) can be derived from Eq.(6):

$$\ln[\sinh(\alpha\sigma_p)] = \ln\dot{\varepsilon}/n - \ln A/n + Q/RTn \quad (9)$$

According to Eqs.(5) and (8), Eqs.(9)~(11) can be got:

$$\left|\partial\ln\dot{\varepsilon}/\partial\ln\left[\sinh(\alpha\sigma p)\right]\right|_T = n \quad (10)$$

$$\left|\partial\ln[\sinh(\alpha\sigma_p)]/\partial(1/T)\right|_{\dot{\varepsilon}} = Q/Rn = n_2 \quad (11)$$

$$Q=R|\partial\ln\dot{\varepsilon}/\partial\ln[\sinh(\alpha\sigma_p)]|_T|\partial\ln[\sinh(\alpha\sigma_p)]/\partial(1/T)|=Rnn_2 \quad (12)$$

Substituting the peak values of flow stress into Eq.(6), the relationships of hyperbolic sine $\ln\dot{\varepsilon}$-$\ln[\sinh(\alpha\sigma_p)]$ and $\ln[\sinh(\alpha\sigma_p)]$-$1/T$ are derived and shown in Fig.10. The average values of n and n_2 are 3.108 and 20.005, respectively. And then the deformation activation energy Q at high temperature can be calculated to be 516.908 kJ·mol^{-1}.

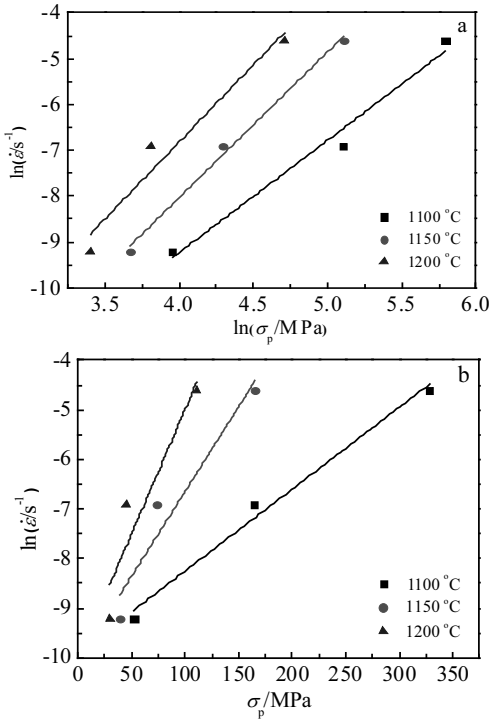

Fig.9 Relationships between the strain rate and peak stress: (a) exponential relationship and (b) power exponential relationship

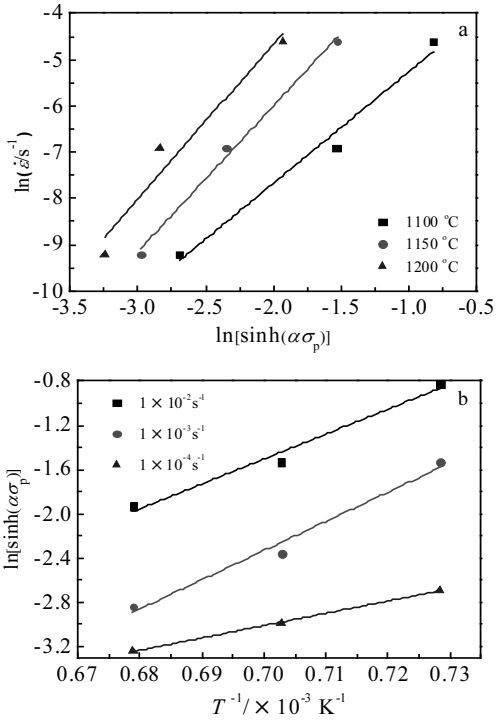

Fig.10 Hyperbolic sine relationship of peak flow stress, strain rate and deformation temperature: (a) $\ln\dot{\varepsilon}$-$\ln[\sinh(\alpha\sigma_p)]$ and (b) $\ln[\sinh(\alpha\sigma_p)]$-$1/T$

As shown in Fig.9 and Fig.10, the experimental data obtained under different deformation conditions are in good agreement with the linear regression equation. Substituting Q value into Eq.(3) and working out Z value, a detailed analysis can be performed by taking the double logarithmic approximation between Z and σ_p. A more precise estimation of n value is obtained through the regression line in Fig.11 $\ln Z$-$\ln[\sinh(\alpha\sigma_p)]$. By substituting this n value into the above equations, a new set of constants A, n, α and Q can be calculated. Iterative calculations carried out in such way are used for more accurate and reliable values.

Fig.11 depicts the relation curve between Z parameters and the peak flow stress after iterative computation for the first time. Table 2 tabulates the values of A, n, m and Q after two regression analyses. Here, m is the strain sensitivity coefficient (m=1/n).

Constitutive equation of Ti-45Al-5Nb alloy during hot compression deformation is derived as:

$$\dot{\varepsilon} = e^{42.670}[\sinh(0.0013\sigma)]^{2.720}\exp(-516908/RT) \quad (13)$$

The above analysis shows that the peak stress- deformation condition of Ti-45Al-5Nb alloy under hot compression deformation satisfies the hyperbolic-sine function relation. Uvira and Jonas have put forward that the value of n is motion of dislocations controlled by climb in the range of 4~5. Nowadays, it is also accepted to be near 3[27]. The value of n is obtained by combining calculation and theory. It is mainly related to equiaxed ultrafine grain/nanocrystalline γ-TiAl+α_2-Ti_3Al two-phase structure. Therefore, the high-temperature deformation mechanism is to be adjusted by climbing of edge dislocations. The strain sensitivity coefficient m is taken as an important index to measure the superplasticity, which indicates the dependence of stress and strain rate on the superplastic deformation of the alloy. The value of the calculated m is 0.37, which is higher than 0.3 ($m \geqslant 0.3$ is required for superplasticity), implying that the superplastic deformation occurs in the materials, where the deformation mechanism is the grain boundary slip. The structure of this study obtained m which is lower than usual[28]. The activation energy obtained by calculation is obviously higher than that for self-diffusion in TiAl alloy (290~345 kJ·mol^{-1})[29]. On the one hand, the deformation activation energy of materials increases due to the fine equiaxial grains. On the other hand, the addition of alloy elements also increases the deformation activation energy[30]. Some researchers have pointed out that dynamic recovery is the dominant deformation mechanism when the activation energy is close to the self-diffusion activation energy. Whereas, dynamic recrystallization is the main deformation mechanism when the activation energy for deformation is much higher than the self-diffusion activation energy.

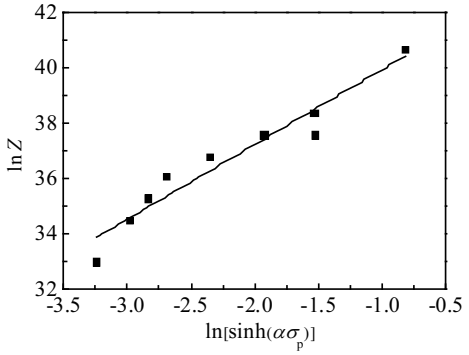

Fig.11 Relation curve of ln$Z$ and ln[sinh($\alpha\sigma$)]

Table 2 Parameter values of the Ti-45Al-5Nb alloy

ln$A$	n	m	α	Q/kJ·mol^{-1}
42.670	2.720	0.370	0.0013	516.908

3 Conclusions

1) The ultrafine and equiaxed microstructure of TiAl-based alloy is obtained by powder ball milling and vacuum sintering. In the range of 1100~1200 °C and strain rate 1×10^{-4}~1×10^{-2} s^{-1}, the alloy can be thermoformed. Compared with the micron-scale structure, the flow stress of the ultrafine/equiaxed microstructure is lower and the peak flow stress is only 30 MPa at 1200 °C, 1×10^{-4} s^{-1}.

2) The peak stress value is reached at the early stage of compression (2.5%~3% strain) achieving the work hardening rapidly. The flow stress decreases with increasing temperature and decreasing strain rate. The deformation activation energy (Q) is 516.908 kJ·mol^{-1} and the stress exponent is 2.720. The constitutive equation is derived as:

$$\dot{\varepsilon} = e^{42.670}[\sinh(0.0013\sigma)]^{2.720}\exp(-516908/RT)$$

3) The deformation mechanism is mainly the dislocation-coordinated deformation of γ-TiAl phase intragranular and γ/γ (001) intergranular deformation twins. Even under the conditions of the high temperature and low strain rate, the microstructure also appears to contain a large number of twins that contribute to deformation.

References

1 Luo Yuanyuan, Zeng Weidong, Xi Zhengping *et al. Rare Metal Materials and Engineering*[J], 2015, 44(2): 282
2 Bean G E, Ebrahimi F, Manuel M V. *Intermetallics*[J], 2014, 49(3): 132
3 Hsiung L M, Nieh T G. *Materials Science & Engineering A*[J], 2004, 364(1-2): 1
4 Equo K, Yoshinao M. *Journal of Japan Institute of Light Metals*[J], 1991, 44(11): 595
5 Hashimoto K, *Journal of Japan Institute of Light Metals*[J], 1994, 44(11): 609
6 Chen Guang, Peng Yingbo, Zheng Gong *et al. Nature Materials*[J], 2016, 15(8): 876

7 Wunderlich W, Kremser T, Frommeyer G. *Acta Metallurgica et Materialia*[J], 1993, 41(6): 1791
8 Sharma G, Joshi K B, Dhaka M S *et al. Intermetallics*[J], 2011, 19(8): 1107
9 Bimal K K, Joshi K B, Dhaka M S *et al*. *Materials Research Society*[J], 1993, 288: 495
10 Xiao Daihong, Yuan Tiechui, Ou Xiaoqin *et al. Transactions of Nonferrous Metals Society of China*[J], 2011, 21(6): 1269
11 Qiu Congzhang, Liu Yong, Zhang Wei *et al. Intermetallics*[J], 2012, 27(3): 46
12 Zan Xiang, He Yuehui, Wang Yang *et al*. *Transactions of Nonferrous Metals Society of China*[J], 2011, 21(1): 45
13 Chu Wuyang, Thompson A W. *Scripta Metallurgica et Materialia*[J], 1991, 25: 641
14 Yokoshima S, Yamaguchi M. *Acta Materialia*[J], 1996, 44(3): 873
15 Kishida K, Inui H, Yamaguchi M. *Intermetallics*[J], 1999, 7: 1131
16 Chen Hua, Zhou Huimin, Zou Yang. *Rare Metal Materials and Engineering*[J], 2015, 44(10): 2387
17 Zou Yang, Zhou Huimin, Chen Hua. *International Conference on Materials Science*[J], 2015, 19: 153
18 Sun Hongfei, Li Xuewen, Feng Jie *et al. Transactions of Nonferrous Metals Society of China*[J], 2012, 22(S2): S491
19 Zhang Peng. *Study on the Microstructure and Properties of Ti-45Al-5Nb Alloy Prepared By Powder Metallurgy*[D]. Harbin: Harbin Institute of Technology, 2013 (in Chinese)
20 Godor F, Werner R, Lindemann J *et al. Materials Science & Engineering A*[J], 2015, 648: 212
21 Liang Cheng, Hui Chang, Bin Tang *et al. Journal of Alloys & Compounds*[J], 2013, 552(9): 364
22 Li Jianbo, Liu Yong, Liu Bin *et al. Intermetallics*[J], 2014, 52: 51
23 Leyens C, Peters M. *Titanium and Titanium Alloys: Fundamentals and Applications*[M]. Beijing: Chemical Industry Press, 2003: 120 (in Chinese)
24 Sellars C M. *Metal Science Journal*[J], 1999, 6(11): 1073
25 Zener C, Hollomon H. *Journal of Applied Physics*[J], 1944, 15(1): 23
26 Uvira J L, Jonas J J. *Transactions of the Metallurgical Society of Aime*[J], 1967, 242(8)
27 He J S, Wang Y W. *Metal Superplasticity*[M]. Beijing: Beijing Science and Technology Press, 1986: 26 (in Chinese)
28 Russell A M, Lee K L. *Structure-Property Relations in Nonferrous Metals*[M]. Hoboken: John Wiley & Sons Inc Press, 2005: 84
29 Herzing C, Przeorsk T, Mishin Y. *Intermetallics*[J], 1999, 7(3-4): 389
30 Xu Wenchen, Shan Debin, Li Chunfeng *et al*. *Journal of Aeronautical Materials*[J], 2005, 25: 14

超细晶/纳米晶 γ-TiAl 基合金的流变行为研究

陈　华，裴　文，宫学博，段振鑫

(长春工业大学，吉林 长春 130000)

摘　要：采用高能球磨及真空热压烧结方法制备超细晶/纳米晶双相 γ-TiAl 基合金。将 Ti、Al、Nb 单质粉末经高能球磨配制成名义成分为 Ti-45Al-5Nb(原子分数, %) 的纳米级混合粉末。球磨后的混合粉末经真空热压烧结（烧结温度 1200 ℃，压力 30 MPa，保温保压 1 h），原位合成 Ti_3Al 及 γ-TiAl 双相等轴状合金组织，烧结组织由小于 500 nm 的等轴 γ-TiAl 相和纳米晶 Ti_3Al 相组成。利用 Gleeble-1500D 对合金进行热压缩模拟实验，变形温度为 1100~1200 ℃、应变速率 1×10^{-4}~1×10^{-2} s^{-1}，研究该合金压缩组织及流变行为。结果表明：与 γ-TiAl 合金微米级晶粒组织相比，超细等轴双相 TiAl+Ti_3Al 组织明显降低了流变峰值应力，使其在2%~2.5%应变量时就达到最大，流变应力随应变速率的降低和温度的升高而降低。同时建立流变应力本构方程，反映一定条件下流变过程中材料的结构特性。结果表明，变形机制主要是在基体 γ-TiAl 相中的位错和 γ/γ(001)的晶间孪晶。

关键词：γ-TiAl 基合金；超细晶/纳米晶；热压缩；本构方程

作者简介：陈　华，女，1963 年生，博士，教授，长春工业大学材料科学与工程学院，吉林 长春 130000，电话：0431-85716396，E-mail: chenhua@ccut.edu.cn